On the bonding and structure of amorphous $Nb_{1-x}Si_x$ films

1989 J. Phys.: Condens. Matter 1 5595

(http://iopscience.iop.org/0953-8984/1/33/002)

J. Phys.: Condens. Matter 1 (1989) 5595–5606. Printed in the UK

On the bonding and structure of amorphous $Nb_{1-x}Si_x$ films

G Wiech†, W Zahorowski†§, A Šimůnek‡ and O Šipr‡

† Sektion Physik, Ludwig-Maximilians-Universität München, Geschwister-Scholl-Platz 1, 8000 München 22, Federal Republic of Germany

‡ Institute of Physics, Czechoslovakian Academy of Sciences, Na Slovance 2, 180 40 Prague 8, Czechoslovakia

Received 15 December 1988

Abstract. The Nb–Si bond and the local structure of the amorphous alloy system $Nb_{1-x}Si_x$ are studied in a wide range of concentrations x: $0.2 \leqslant x \leqslant 0.8$. The experimental approach is provided by x-ray emission spectroscopy, x-ray photoelectron spectroscopy and x-ray diffraction measurements. The electronic properties and the bonding interaction between Nb and Si atoms are investigated for hypothetical Nb–Si structures by self-consistent pseudopotential calculations. A detailed analysis of all experimental data is given. It is found that the silicon short-range order changes considerably within the concentration interval $0.50 < x < 0.57$. The comparison of the results obtained for the system $Nb_{1-x}Si_x$ with x-ray spectra of crystalline Nb_5Si_3 and $NbSi_2$ implies that in the metallic phases of $Nb_{1-x}Si_x$ for $0.2 \leqslant x \leqslant 0.8$ the coordination of Si is other than tetrahedral.

1. Introduction

The central point at issue which must be studied for systems which do not have long-range periodicity is the local structure. Knowledge of the local structure is a necessary prerequisite for the understanding of the physical properties of complex materials which can form systems in a continuous range of concentrations. First, there is the natural question about the local structure of amorphous alloys with concentrations at which no crystalline counterpart exists. However, even for concentrations at which crystalline phases of the same composition are available, the local structure of the amorphous phase is a matter of considerable interest; very often amorphous alloys exhibit an uncommon combination of various physical properties not encountered in the crystalline analogues. In the present work, we have undertaken experimental and theoretical studies to correlate the electronic structure with the local structure of amorphous films of the alloy system $Nb_{1-x}Si_x$ (a-$Nb_{1-x}Si_x$) in a wide range of concentrations, x: $0.2 \leqslant x \leqslant 0.8$.

Transition-metal silicides, with their wide variety of structures and electronic properties, are of great current interest, largely because of microelectronic device applications. The system a-$Nb_{1-x}Si_x$ existing in the wide range of concentrations $0 \leqslant x \leqslant 1$ changes its electronic properties from metallic to semiconducting behaviour. The films form crystalline metals for $x \leqslant 0.13$, amorphous metals for $0.15 \leqslant x \leqslant 0.85$ and amorphous semiconductors for $x \geqslant 0.87$ [1].

§ On leave from the Institute of Physics, Polish Academy of Sciences, 02668 Warsaw, Poland.

0953-8984/89/335595 + 12 $02.50

In an earlier investigation the electronic structure of a-$Nb_{1-x}Si_x$ was studied by x-ray emission spectroscopy (XES) and x-ray photoelectron spectroscopy (XPS) and the experimental valence band spectra have been reported [2, 3]. The aim of the present paper is to investigate the local structure of a-$Nb_{1-x}Si_x$. As the electronic states of a solid are inherently bound to its local structure, we have performed self-consistent band-structure calculations for hypothetical Nb–Si compounds in various high-symmetry structures. The calculated local densities of states are correlated with measured XES and XPS spectra of a-$Nb_{1-x}Si_x$ and the observed spectral changes dependent on the composition parameter x are analysed.

Both XPS and XES techniques enable us to investigate the electronic structure within the whole energy range of the valence states; however, different transition probabilities for these experimental techniques differently exhibit Si and Nb electrons in the measured spectra. As a consequence of the dipole selection rules the x-ray K emission bands and the L emission bands reflect local p-like and s-and/or d-like electronic states, respectively. On the other hand, the photoemission cross sections σ at Al Kα energy ($h\nu = 1486.6$ eV [4])

$$\sigma(\text{Nb 4d}) \simeq \sigma(\text{Si 3s}) \gg \sigma(\text{Si 3p})$$

suppress the Si 3p states observable in the Si K emission bands. In the system a-$Nb_{1-x}Si_x$ the binding energies of the Nb 4d, Si 3s and Si 3p electrons are different and consequently the corresponding features in the XPS and XES spectra are well separated. As a result of XPS and XES matrix element effects and the natural binding energy separation of s, p and d electrons, XES and XPS yield complementary experimental data for Nb–Si compounds.

To obtain more insight into the structural aspects of our spectroscopic results, we present also Si K emission bands of crystalline Nb_5Si_3 and $NbSi_2$. Finally we discuss the x-ray diffraction measurements of a-$Nb_{1-x}Si_x$ [5] which provide additional experimental data for the structure analysis. In § 2, we shall briefly report sample preparation and some technical details of the experiments and the self-consistent pseudopotential calculations. In § 3 the observed XPS and XES spectra are described in detail and the results of the electronic structure calculations are presented. In the final section, § 4, the results are discussed and an interpretation and conclusions are given.

2. Experimental and theoretical techniques

2.1. Experiment

The a-$Nb_{1-x}Si_x$ alloy films were prepared by co-sputtering using Si and Nb targets [3]. The samples for the XPS and XES measurements were deposited on sapphire substrates (thickness, 0.15–0.45 μm) and on copper substrates (thickness, 1–4 μm), respectively. The structure of the films was studied by x-ray diffraction, and the sample composition by Rutherford back-scattering. The details of sample preparation, sample analysis and the XPS measurements have been fully described in [3, 6]. Therefore we present here only the most relevant facts.

After preparation the thin-film samples were transferred to the analysing chamber of a Leybold EA10-100 analyser without breaking the vacuum. The valence band features were measured by taking the electron energy distribution curves at the photon energy of unmonochromated Al Kα radiation (1486.6 eV) and a total resolution of about 1.5 eV. The XES spectra were measured with a Johann-type spectrometer applying

fluorescence excitation(W anode; 10 kV, 200 mA). The pressure in the spectrometer and the x-ray tube was less than 1×10^{-5} Torr. The dispersing element was a quartz crystal cut parallel to $10\bar{1}0$ and bent to a radius of 108 cm. The total resolution was about 0.6 eV. First, all XES spectra were recorded with a flow-proportional counter (Ar–methane) operated at atmospheric pressure. The spectra were recorded automatically in the step-scanning mode. The measuring time for one spectrum was about 3 h. To obtain an intensity of about 6000 counts in the maximum of the Si K emission bands, eight spectra had to be accumulated for a-Si and 40 for a-$Nb_{0.80}Si_{0.20}$. No changes in the spectra were observable during the measurements, indicating that the samples remained unchanged. The Si K emission band of $NbSi_2$ (see figure 8) was measured with the same spectrometer and the experimental conditions were completely comparable with those for the amorphous films.

When a position-sensitive detector (which had been developed in our laboratory) became available, some of the Si K emission bands ($x = 0.20$, 0.50 and 0.80) were remeasured with considerably improved statistics using new samples. Compared with the above-mentioned flow-proportional counter a gain in time by a factor of 20 or more was obtained. The spatial resolution of the system consisting of the detector and the crystal is less than 200 μm (comparable with the slit width of 200 μm when the step-scanning mode was used). The position-sensitive detector has a backgammon geometry of one of its two cathodes. The results obtained with this detector are virtually identical with the earlier measurements [3], except for the much better statistics.

2.2. Theory

The calculated *l*-decomposed density of states presented for crystalline NbSi (CsCl crystal structure) and crystalline $NbSi_3$ (Cu_3Au crystal structure) were derived from energy band calculations employing the local-density approximation and the Hedin–Lundqvist form of the exchange correlation energy [7]. The pseudopotential approach for the solution of the effective one-electron equation was applied and the *ab initio* pseudopotentials of Nb and Si were used [8]. The calculations are self-consistent; the only inputs were the structure type and the atomic spacing. As spin–orbit coupling has little effect on the band structure of $MoSi_2$ [9], the spin–orbit interaction is neglected in our computation.

3. Results

3.1. Alignment of photon energy and binding energy scales

The XPS spectra, the Si K and Nb L emission bands of the a-$Nb_{1-x}Si_x$ films for $0.20 \leqslant x \leqslant 1.0$ are presented later in figures 1, 2 and 4. In each figure the peak heights of all spectra are adjusted to the same value. The energies of the XPS valence band spectra and the XES emission bands of different composition parameters x are related to the binding energy and the photon energy scales, respectively.

We correlated Nb L and Si K photon energy scales with the XPS binding energy scale by making use of the XES selection rules and the XPS cross sections in the following way.

(i) The Nb L emission band and the XPS spectrum of a-$Nb_{0.80}Si_{0.20}$ reflect Nb 4d-like states. We therefore placed the maxima of both spectra at the same energy position.

The photon energy of 2367.2 eV for the Nb L emission band then corresponds to the zero of the scale of binding energies determined by XPS.

(ii) The Si L emission band and the XPS spectrum of amorphous silicon (a-Si) reflect Si s-like states. The mutual correspondence of features in both spectra indicates that the photon energy of 99.3 eV coincides with the zero of the XPS binding energy scale.

The spectra aligned according to (i) and (ii) are presented in figures 1 and 2, respectively. Since the Si L and Si K emission bands of a-Si can be correlated with the Si Kα lines [10], all Si K emission band photon energies of the alloy system a-$Nb_{1-x}Si_x$ are related to the XPS binding energy scale; the photon energy of 1839.2 eV coincides with the zero mark of the binding energy scale. For all concentrations x the binding energies of Si s-like valence states determined from XPS are the same (8.4 eV). Since these states are involved in the bond and have an atomic-like character (see § 4), we assume the energy position of the deeper core levels of silicon to be independent of the concentration as well. Consequently the photon energy scale is fixed relative to E_F for all concentrations under study.

The alignment of XES and XPS spectra as described in the preceding paragraphs has been applied in figures 1, 2 and 4. In all figures and in the following text the features and peaks of spectra will be discussed with reference to the binding energy scale. The XES spectra represent the original measurements with a linear background subtracted; the XPS spectra are original data with no background subtraction.

3.2. XES and XPS valence band spectra

In figure 1, we present the XPS spectra and the Nb L emission bands for the $Nb_{0.8}Si_{0.2}$ and $Nb_{0.2}Si_{0.8}$. In going from $Nb_{0.8}Si_{0.2}$ to $Nb_{0.2}Si_{0.8}$ the main peak of the XPS spectra shifts from 1.4 to 2.1 eV, but the position of a feature at 8.4 eV remains unchanged for both compositions. The Nb L emission bands reflect Nb 4d electrons. By comparing the niobium-rich with the niobium-deficient sample, we note that the peak of the Nb L band is shifted from 1.4 to 1.0 eV and broadens from 3.7 to 4.2 eV (full width at half-maximum (FWHM)).

The feature at 8.4 eV in the XPS spectra indicates the position of the Si 3s electrons. Its intensity rises with increasing x, i.e. with increasing Si concentration. In the Nb L emission bands, no feature corresponding to this can be observed.

In figure 2, we present XPS and Si K emission spectra of a-$Nb_{1-x}Si_x$ for $0.2 \leqslant x \leqslant 1.0$. The L emission band of a-Si is included (full curve in the lowest part of figure 2). The XPS spectrum for $x = 0.4$ is similar to that for $x = 0.2$; the peaks of both spectra are at almost the same energies. The XPS spectra for $x = 0.6$ and $x = 0.8$ are similar to each other as well. Accordingly the shift of the main peak and the broadening of the XPS spectra (figure 1) is to be attributed to the interval of concentrations $0.4 < x < 0.6$. The Si K emission bands reflecting Si p electrons exhibit a main peak at 4.1 eV and a shoulder on the high-binding-energy side of the peak at 7.8 eV. Both features do not change their energy positions within $0.2 \leqslant x \leqslant 0.8$; the widths of the emission bands, however, increase significantly. In figure 3 the FWHM values are presented for our old and new XES measurements. As can be seen from figure 2, the FWHM values arise particularly as a result of an enhancement of intensity at low binding energies ($E < 4.1$ eV). The main peak of the Si K emission band of a-Si is located in this energy range. This figure also shows the remarkable similarity of the XPS spectrum and the Si L emission band of a-Si.

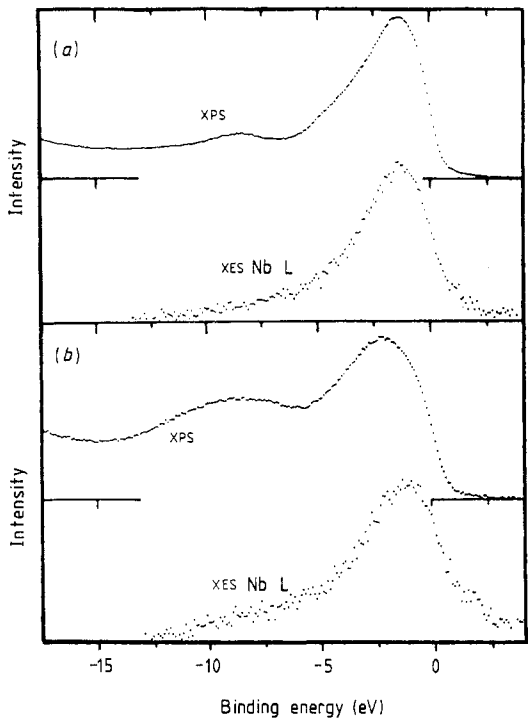

Figure 1. XPS spectra and Nb Lβ emission bands of a-$Nb_{1-x}Si_x$ for (*a*) $x = 0.20$ and (*b*) $x = 0.80$.

The positions of peaks and features are the same for all XES spectra and the main changes occur at low binding energies (0 eV $< E <$ 4.1 eV). These changes in the spectral shapes are associated with an increase in the FWHM. It is remarkable that the FWHM changes drastically (by about 0.9 eV) within the small range of concentrations $0.50 \leqslant x \leqslant 0.57$ while between $x = 0.35$ and $x = 0.50$ and between $x = 0.57$ and $x = 0.65$ the changes are much smaller (less than 0.2 eV). The sudden reshaping of the spectrum with x is clearly demonstrated in figure 4.

3.3. X-ray diffraction data

X-ray diffraction data of the system a-$Nb_{1-x}Si_x$ were published in [5]. Figure 5 shows the x-ray diffraction spectra for $x = 0.2, 0.4, 0.6, 0.8$ and 1.0 (a-Si). The spectra exhibit a non-gradual development of features in going from $x = 0.2$ to $x = 1.0$. There are two distinct features in the spectra for $x = 0.2$ and $x = 0.4$: a main peak at an angle θ (which is half the diffraction angle) of 19–20° and a smaller peak at about 33°. The spectra for $x = 0.6$ and $x = 0.8$ are different from the previous ones but are again similar to each other. There are three features: the main peak again at 19–20°; a smaller peak at about 31.5° and a new feature at about 14°. The diffraction spectrum of a-Si differs considerably from all previous spectra. Its main peak is at 14.5°, and there is a shoulder at about 26.5°.

3.4. Model band-structure calculations

The complex structure of real crystalline niobium silicides Nb_3Si, Nb_5Si_3 and $NbSi_2$ has hindered calculations of their electronic structures. At present, no energy band

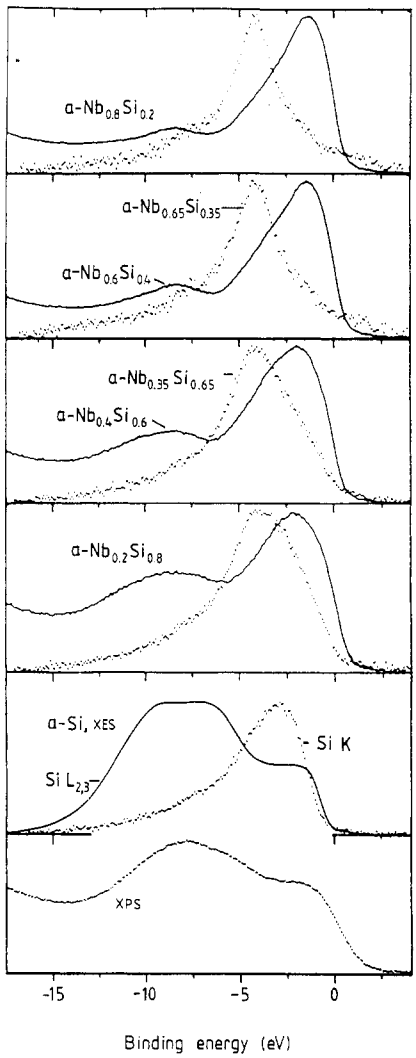

Figure 2. XPS spectra (——) and Si K emission bands (·····) of a-$Nb_{1-x}Si_x$ for various compositions x ($0.2 \leq x \leq 0.8$). In the lowest part the Si K and Si L emission bands and the XPS spectrum of a-Si ($x = 1.0$) are displayed.

calculations for any Nb–Si crystals are available to us. To find some common aspects of the Nb–Si bond in real crystals, we recall the shortest inter-atomic distances in these crystals. In Nb_3Si (Ti_3P structure, $P4_2/n$) [11] the shortest inter-atomic distances d are d(Nb–Si) = 2.58 Å, d(Nb–Nb) = 2.64 Å and d(Si–Si) = 3.78 Å. In Nb_5Si_3 (Cr_5B_3 structure; I4/mcm) [12], we have the distances d(Nb–Si) = 2.59 Å, d(Nb–Nb) = 3.02 Å and d(Si–Si) = 3.94 Å; in $NbSi_2$ ($CrSi_2$ structure; $P6_222$) [13] the corresponding distances are d(Nb–Si) = 2.59 Å, d(Nb–Nb) = 3.24 Å and d(Si–Si) = 2.59 Å. In all three silicides the Nb–Si distances are almost the same; the Nb–Nb and Si–Si distances, however, differ essentially. It is interesting to note here that the half-bonding distances s in the crystals of pure Si and pure Nb are s(Si) = 1.17 Å and s(Nb) = 1.43 Å, respectively, and that

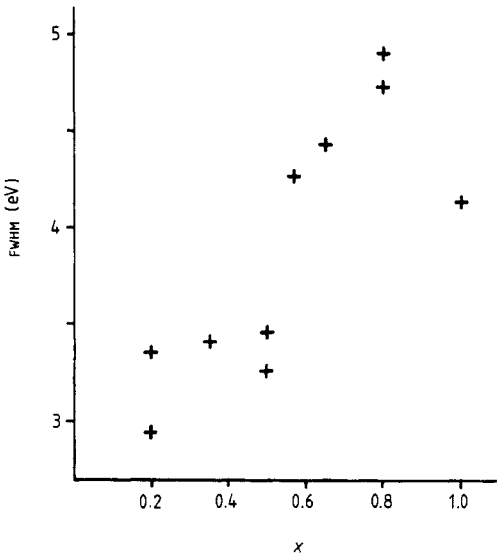

Figure 3. FWHM of Si K emission bands against sample composition parameter x.

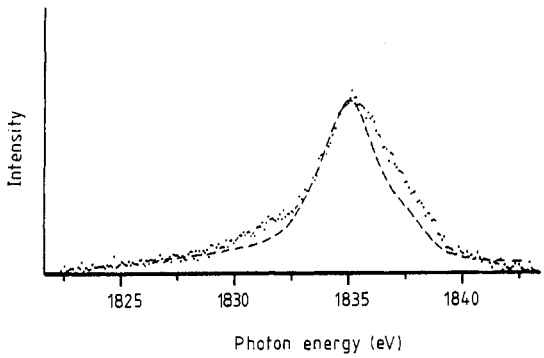

Figure 4. Si K emission bands of a-$Nb_{1-x}Si_x$ for $x = 0.50$ (– – –) and $x = 0.57$ (· · · · ·).

their sum s(Si) + s(Nb) = 2.60 is in good accordance with the d(Nb–Si) distances in the Nb–Si crystals.

Since the distances d(Nb–Si) are almost the same for the real crystals, it seems reasonable to use the value of 2.60 Å also for the atomic Nb–Si distance in our calculations. To study the consequences of the local geometry on the partial density of states, we calculated the band structures of Nb–Si model crystals with CsCl, NaCl, Cu_3Au and ZnS structures. A similar approach was practiced in [14] for 3d transition-metal disilicides. It was found that the observed general trends of chemical bonding are adequately described by model calculations employing the augmented-spherical-wave procedure to the cubic CuAu and Cu_3Au structures.

Our calculations based on cubic CsCl (for NbSi) and Cu_3Au (for $NbSi_3$) provide results relevant to the experimental XPS and XES data. The theoretical results for NaCl and ZnS structures cannot be adequately compared with the measured spectra, and therefore we do not present them here. The calculated l-decomposed local density of states for NbSi (CsCl) and $NbSi_3$ (Cu_3Au) are shown in figure 6 and figure 7, respectively.

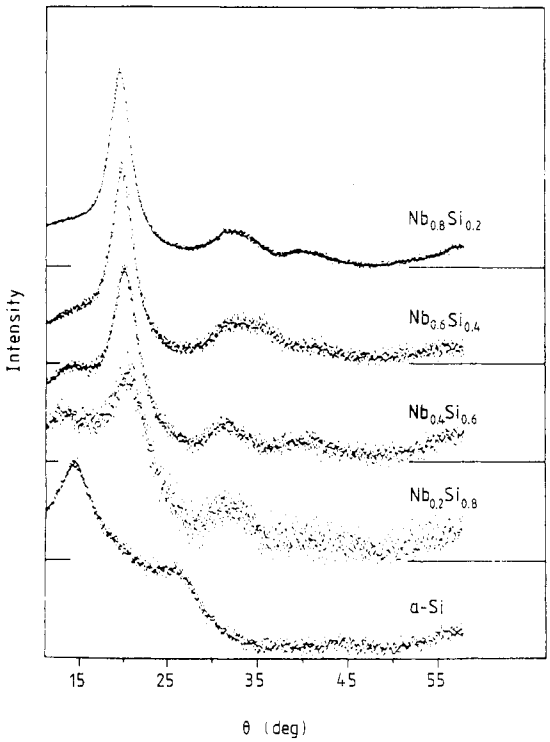

Figure 5. X-ray diffraction curves of a-$Nb_{1-x}Si_x$ for $x = 0.2, 0.4, 0.6, 0.8$ and 1.0 (a-Si) taken from [5].

As can be seen, the centres of the s, p and d states are clearly separated and they are at similar energy positions to those in the spectroscopic results. The Si s states are centred at approximately 8–9 eV, the Si p states at approximately 4–5 eV and the Nb d states near the Fermi energy and extending to about 5 eV. These results are in good qualitative accordance with general trends observed in calculations in [14–16].

4. Discussion and conclusions

In the XES and XPS spectra of a-$Nb_{1-x}Si_x$, we observe three distinct and dominant features at binding energies of 8.4 eV, 4.1 eV and 1–2 eV, respectively, in figure 2, which are closely related to particular bonds.

The valence Si s electrons forming peaks at 8.4 eV are not involved in the bond, remaining in a quasi-atomic configuration, which for instance can be discerned from figures 6 and 7 and from [14]. The Si p electrons form the peaks at 4.1 eV, their position being stable for all x in the composition interval $0.2 \leqslant x \leqslant 0.8$, and the Nb d electrons create the peaks with maxima at 1–2 eV. For crystalline silicides, it has been shown [14] that the bonding mixture of Si 3p and 3d transition-metal electrons (p–d bond) accounts for the stability of the silicides. The p and d electrons hybridise to form a bonding hybrid which is more tightly bound than either of the states from which it originally formed [17]. The good knowledge of p–d bonds in crystalline 3d transition-metal silicides and

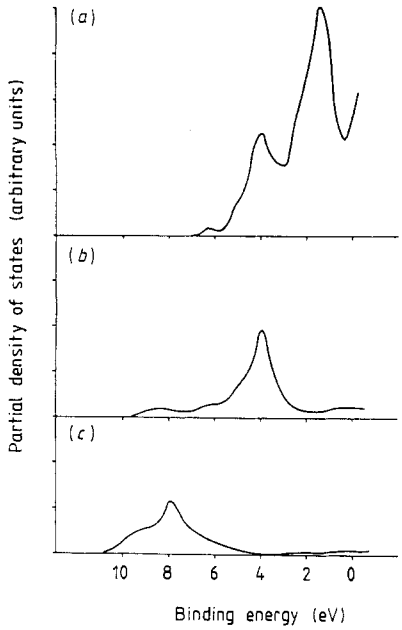

Figure 6. Calculated partial densities of states for NbSi in the CsCl crystal structure; (*a*) Nb d; (*b*) Si p; (*c*) Si s. The same units for the s, p and d densities are used.

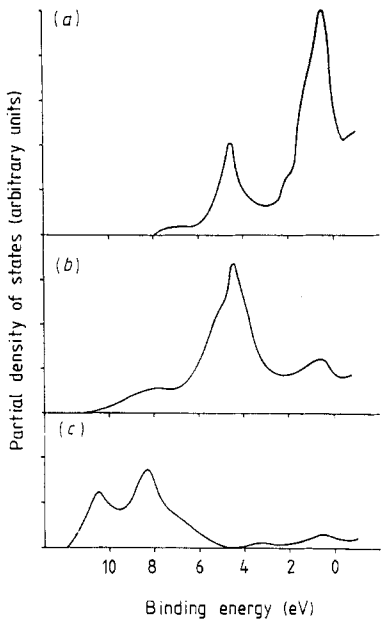

Figure 7. Calculated partial densities of states for $NbSi_3$ in the Cu_3Au crystal structure; (*a*) Nb d; (*b*) Si p; (*c*) Si s. The same units for s, p and d densities are used.

the spectroscopic measurements of Nb–Si crystals form a base for our analysis of the p–d bonds in the amorphous system $Nb_{1-x}Si_x$.

We have realised that for the concentrations $x \leqslant 0.5$ the Si K emission bands are very similar to the Si K emission band of crystalline Nb_5Si_3 [18]. All these spectra exhibit a 'triangular' shape (see figure 2, where there is almost no asymmetry of the spectral curves, the same energy positions of the band maxima and a comparable FWHM, which is 2.9 eV for Nb_5Si_3). It is noteworthy and probably significant that the Si atoms in Nb_5Si_3 (Cr_5B_3-type structure) are surrounded by 10 nearest-neighbour Nb atoms in square-planar configurations [11]. It is remarkable that the square-planar configuration is retained also in Nb_3Si (Ti_3P-type structure) [11], taking into account the competition with the packing requirement of the Nb atoms, which constitute a 75% majority. The fact that Nb–Si bonding interactions predominate even in the case of low Si content suggests that

(i) this is true also for amorphous silicides and

(ii) the local structure around the Si atoms for $x \leqslant 0.5$ is of similar square-planar character.

For the concentration range $0.57 \leqslant x \leqslant 0.8$, we compare the Si K emission bands of a-$Nb_{1-x}Si_x$ with that of crystalline $NbSi_2$ [19]. In figure 8 the Si K emission bands of $NbSi_2$ and a-$Nb_{0.35}Si_{0.65}$ (which is comparable with $NbSi_2$ in composition) are shown. The Si K emission band of $NbSi_2$ exhibits three distinct features: the main maximum γ at 1836.9 eV, a shoulder β at 1835.0 eV and a low-intensity peak α at 1831.8 eV (binding energies of 2.3 eV, 4.2 eV and 7.4 eV, respectively). The origin of these peaks can be

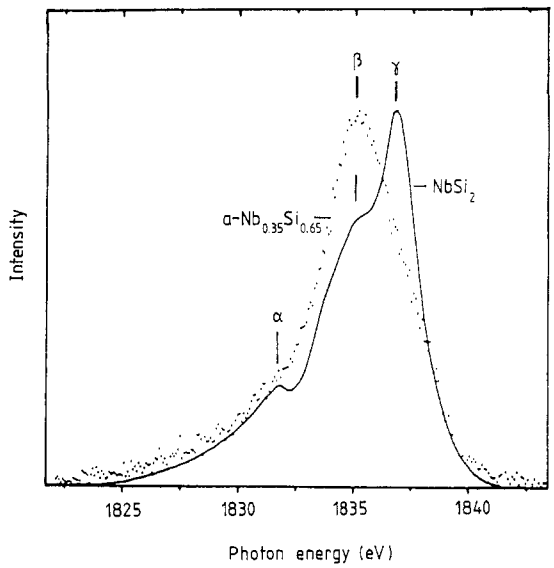

Figure 8. Si K emission bands of crystalline $NbSi_2$ (taken from [19]) and a-$Nb_{0.35}Si_{0.65}$.

interpreted using structural and spectroscopic analogies with $CrSi_2$ and $MoSi_2$ studied theoretically [9, 15] and also experimentally by XES and XPS techniques [20]. As shown in figure 8, the Si 3p states of $NbSi_2$ are split into two main features β and γ; peak α consists of the Si s–p hybrid. The shoulder β arises from strong Nb-Si d–p bonds, while the narrow peak γ reflects Si p electrons. Contrary to the case for $NbSi_2$, the Si 3p states in a-$Nb_{1-x}Si_x$ are not split into two features. The energy position of β in $NbSi_2$ coincides with the maximum of a-$Nb_{0.35}Si_{0.65}$; however, where the main maximum γ of $NbSi_2$ is observed, the intensity in the Si K emission band of a-$Nb_{0.35}Si_{0.65}$ decreases without any notable feature. These spectral differences express different Si p-like partial densities of states, display the tighter p bond in amorphous than in crystalline $NbSi_2$ and consequently indicate that the local structure in amorphous $Nb_{0.35}Si_{0.65}$ is different from that in the crystalline counterpart $NbSi_2$. In $NbSi_2$ ($CrSi_2$ structure) the Si atom is tetrahedrally surrounded by two Si and two Nb atoms at a distance of 2.59 Å. This tetrahedral coordination is slightly distorted, and another six atoms (three Nb and three Si) at a distance of 2.76 Å [13] may contribute to the Si bonds in $NbSi_2$.

Our band-structure model calculations are in qualitative accordance with the experimental data of the amorphous system $Nb_{1-x}Si_x$ ($0.6 \leqslant x \leqslant 0.8$) only for the two structural models NbSi (figure 6) and $NbSi_3$ (figure 7). The model calculations for the NaCl- and ZnS-type structure do not yield partial densities adequately comparable with the experimental data.

The comparison of the Si spectra of a-$Nb_{1-x}Si_x$, those of the crystalline Nb–Si and $MoSi_2$ compounds and of our model calculations suggests that Nb–Si bonds in non-tetrahedral geometry dominate even for high Si content. The influence of Si–Si bonds does not substantially alter the character of the Si spectra of the amorphous system for x up to 0.8. It seems that the square-planar neighbourhood existing in Nb_5Si and Nb_3Si crystals is preserved, with some variations.

The invariable energy positions of the maximum of the XES spectra (figure 2) for all concentrations in the range $0.2 \leqslant x \leqslant 0.8$ confirm the strength of the p–d bond in the

system a-$Nb_{1-x}Si_x$. If we take into account firstly the coincidence of the energy positions of these maxima with that of the maximum of the Si K emission band of Nb_5Si_3 and secondly the fact that the Nb–Si inter-atomic distances are almost the same in the crystalline silicides Nb_3Si, Nb_5Si_3 and $NbSi_2$ having different structures, we infer that, also in the system a-$Nb_{1-x}Si_x$, the distances between Nb and Si atoms are more or less the same, i.e. about 2.60 Å.

Comparing all XES curves in figure 2, we can observe that at binding energies higher than that of maxima at 4.1 eV the spectra remain more or less unchanged in the whole range $0.2 \leqslant x \leqslant 0.8$. Changes occur only on the low-binding-energy side of the maxima and they can be characterised by the FWHM. As x increases up to $x = 0.5$, the FWHM increases only from about 3.2 eV ($x = 0.2$) to about 3.4 eV ($x = 0.5$). The Nb–Si bond is dominant and Si–Si bonds are of minor importance. Between $x = 0.50$ and $x = 0.57$ the intensity in the low-binding-energy range and also the FWHM increase considerably from about 3.4 to about 4.3 eV. For higher values of x the FWHM does not change as abruptly as in this narrow interval (see figures 3 and 4). It seems that there exists a critical concentration x within the interval $0.50 \leqslant x \leqslant 0.57$ at which the Si p-like partial density of states is substantially changed. Therefore it is quite plausible to expect that at concentrations $x = 0.54 \pm 0.04$ the short-range order in a-$Nb_{1-x}Si_x$ is also altered. This expectation is supported by the x-ray diffraction curves for $x = 0.4$ and $x = 0.6$ in figure 5. Compared with the diffraction curve for $x = 0.4$, that for $x = 0.6$ exhibits a new feature (at about 14°) and the feature at about 32° is shifted to smaller angles.

The intensity I of the x-ray diffraction curves (figure 5) can be described by the Debye scattering equation

$$I(s) = \sum_i \sum_j \frac{f_i f_j \sin(sr_{ij})}{sr_{ij}}$$

where f_i and f_j are the scattering factors of atoms i and j; r_{ij} is the inter-atomic distance of atoms i and j; $s = (4\pi/\lambda) \sin\theta$ and 2θ is the angle between the incident beam and the scattered beam directions. The intensity $I(s)$ of the diffracted beam is given as the sum of oscillating terms $[\sin(sr)]/sr$ summed over all atoms and all inter-atomic distances in the sample. If the contributions to the sum with a particular distance r_d predominate over all the other terms, then the maximum of the function $[\sin(sr_d)]/sr_d$ forms the first and most intense peak in the diffraction curve. The function $[\sin(sr)]/sr$ for $sr \neq 0$ has its first maximum at $sr = 7.725$. Applied to the distance r_d the first peak of the diffraction curve satisfies the equation

$$sr_d = 7.725.$$

In figure 5 the diffraction curves for $x = 0.2$ and $x = 0.4$ indeed exhibit very intense first peaks at 19–20°. For $\theta = 19.3°$ and $\lambda = 1.542$ Å (Cu Kα), we obtain $r_d = 2.86$ Å. This distance is identical to the inter-atomic distances in BCC Nb; that is, in the Nb-rich samples of a-$Nb_{1-x}Si_x$ the inter-atomic distances of the Nb atoms are very similar to those in BCC Nb. According to the different scattering factors of the Nb and Si atoms the smaller Nb–Si distance does not show up in the diffraction curves but slightly moves the diffraction peaks to larger θ for increasing x.

The diffraction curves for $x \geqslant 0.6$ (figure 5) cannot be interpreted in this simple way. Anyhow, the differences between the two groups of curves ($x = 0.2$ and 0.4 and $x = 0.6$ and 0.8) reflect the different short-range orders of atoms in these groups.

These features of the diffraction curve of a-Si ($x = 1.0$) (figure 5) are not compatible with the features of the curves for $x \leqslant 0.8$, and therefore tetrahedal coordination of the

Si atoms in a-$Nb_{1-x}Si_x$ seems improbable. This inference is also supported by our model structure calculations of NbSi with ZnS-type structure. The resulting *l*-decomposed density of states does not exhibit features characteristic of the XES and XPS experimental curves for $x \leqslant 0.8$. It therefore is coherent to assume that the coordination of the Si atoms in a-$Nb_{1-x}Si_x$ evolves into the tetrahedral geometry of a-Si within the interval $0.85 < x < 0.90$, where the transition from metallic to semiconducting behaviour also occurs [1].

Acknowledgments

WZ thanks the German Federal Minister for Research and Technology for financial support which enabled him to work in Munich. Part of the equipment used for the experimental work was funded by Deutsche Forschungsgemeinschaft.

References

[1] Hertel G, Bishop D J, Spencer E G, Rowell J M and Dynes R C 1983 *Phys. Rev. Lett.* **50** 743
[2] Zahorowski W, Šimůnek A, Wiech G, Söldner K, Knauf R and Saemann-Ischenko G 1987 *J. Physique Coll.* **48** C9 1205
[3] Söldner K, Grassmann A, Saemann-Ischenko G, Zahorowski W, Šimůnek A and Wiech G 1989 *Z. Phys.* B **75** 59
[4] Yeh J J and Lindau I 1985 *At. Data Nucl. Data Tables* **32** 1
[5] Söldner K and Saemann-Ischenko G 1987 *Japan. J. Appl. Phys.* **26** 807
[6] Söldner K 1987 *Thesis* Universität Erlangen
[7] Hedin L and Lundqvist B I 1971 *J. Phys. C: Solid State Phys.* **4** 2064
[8] Hamann D R, Schlüter M and Chiang C 1982 *Phys. Rev.* B **26** 4199
[9] Tang Shaoping and Zhang Kaiming 1988 *J. Phys. C: Solid State Phys.* **21** 1469
[10] Kurmaev E Z and Wiech G 1985 *J. Non-Cryst. Solids* **70** 187
[11] Waterstrat R M, Yvon K, Flack H D and Parthe E 1975 *Acta Crystallogr.* B **31** 2765
[12] Parthe E, Lux B and Nowotny H 1977 *Monatsh. Chem.* 108
[13] *Structure Reports* 1944 **8** 102
[14] Weaver J H, Franciosi A and Moruzzi V L 1984 *Phys. Rev.* B **29** 3293
[15] Franciosi A, Weaver J J, O'Neill D G, Schmidt F A, Bisi O and Calandra C 1983 *Phys. Rev.* B **28** 7000
[16] Weaver J H, Moruzzi V L and Schmidt F A 1981 *Phys. Rev.* B **23** 2916
[17] Gelatt C D Jr, Williams A R and Moruzzi V L 1983 *Phys. Rev.* B **27** 2005
[18] Mitternacht J 1988 *Diplomarbeit Universität* München
[19] Zöpf E 1972 *Thesis* Universität München
[20] Sénémaud C, Vergand F, Bonelle C, Thomas O, Sénateur J P and Madar R 1987 *Solid State Commun.* **64** 129